

Why does the intermediate polar V405 Aurigae show a double-peaked spin pulse?

P.A. Evans^{*} and Coel Hellier

Astrophysics Group, School of Chemistry and Physics, Keele University, Staffordshire, ST5 5BG

Accepted Received

ABSTRACT

V405 Aurigae is an intermediate polar showing a double-peaked pulsation in soft X-rays and a single-peaked pulsation in harder X-rays. From *XMM-Newton* observations we find that the soft band is dominated by blackbody emission from the heated white-dwarf surface. Such emission is at a maximum when either magnetic pole points towards us, explaining the double-peaked pulsation. The symmetry of the pulses requires that the angle between the magnetic and spin axes be high.

The single-peaked pulsation in harder X-rays is explained in the usual way, as a result of opacity in the accretion curtains. However, the high dipole inclination means that the accretion curtains are nearly in the plane. Thus the outer regions of the curtains do not cross the line of sight to the accretion footprints, explaining the absence of the deep absorption dip characteristic of many intermediate polars. The sawtooth profile of this pulsation requires that the magnetic axis be offset from the white-dwarf centre.

We remark also on the double-peaked optical emission in this star. We suggest that the difference between V405 Aur's spin pulse and those of other intermediate polars is the result of its high dipole inclination.

Key words: accretion, accretion discs – stars: individual: V405 Aur (RX J0558.0+5353) – novae, cataclysmic variables – X-rays: binaries.

1 INTRODUCTION

V405 Aurigae (RX J0558.0+5353) was discovered in the *Rosat* All-Sky Survey and identified as an intermediate polar (a cataclysmic variable with a magnetic white-dwarf primary) by Haberl et al. (1994).

It is notable, firstly, for showing a soft blackbody component in the X-ray spectrum, one of a number of such objects discovered with *Rosat*. Secondly, its soft-X-ray and optical emission shows a double-peaked modulation at the white-dwarf spin period (e.g. Allan et al. 1996), whereas most of these stars show a single-peaked modulation (see, e.g., Patterson 1994 or Hellier 2001 for reviews of this class).

The hard X-ray emission in intermediate polars (IPs) originates below a stand-off accretion shock near the magnetic poles of the white dwarf. The soft blackbody emission is then understood as arising from heated white-dwarf surface around the accretion footprints. This is nearly always seen in the AM Her class of cataclysmic variable, but it is seen only in some IPs, for which the reason is unclear.

The issue of why some IPs show a single-peaked pulsation, whereas others show a double-peaked pulsation, is also

unclear. One idea (e.g. Hellier 1996; Allan et al. 1996; Norton et al. 1999) notes that IPs with shorter spin periods will have smaller magnetospheres in which the accretion discs are disrupted nearer the white dwarf. This could result in shorter, fatter ‘accretion curtains’ of material which might have lower opacity in the vertical direction, thus preferentially beaming X-rays along magnetic field lines. The two magnetic poles would combine to produce a double-peaked pulsation. With longer spin periods, where disc disruption occurs further out, the opposite might hold, with tall, thin accretion curtains preferentially beaming X-rays out of the sides. The two poles would then act in phase, producing a single-peaked pulsation.

The *XMM-Newton* X-ray satellite has a larger collecting area and better spectral resolution than *Rosat*, allowing us to return to V405 Aur with better X-ray data than previously obtained. We report here on a 30-ks *XMM-Newton* observation aimed at understanding the pulsation at the 545-s spin period of V405 Aur.

^{*} pae@astro.keele.ac.uk

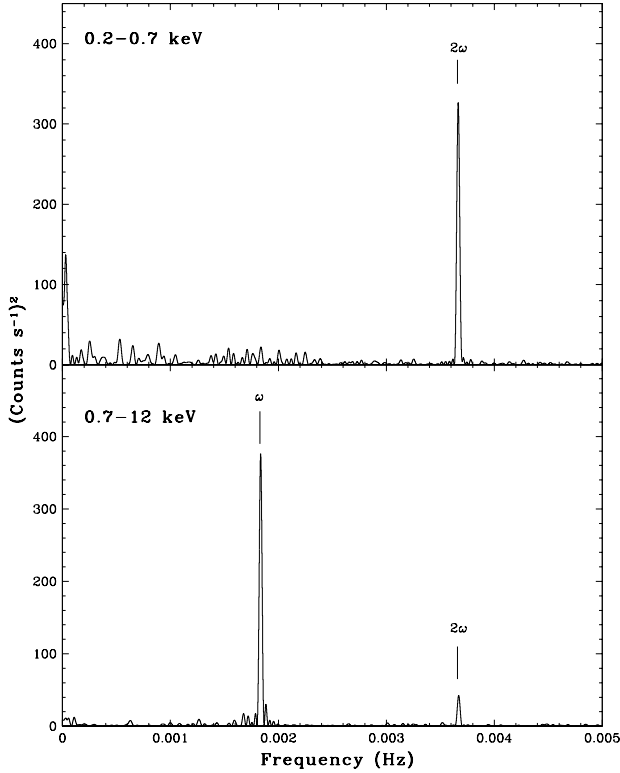


Figure 1. Power spectra of the X-ray data (MOS-1 + MOS-2) in the soft (upper panel) and hard (lower panel) energy bands.

2 OBSERVATIONS AND LIGHTCURVES

V405 Aur was observed by the *XMM-Newton* satellite (Jansen et al. 2001; Turner et al. 2001) on 2001 October 5. A 30-ks observation was made with the EPIC-MOS cameras in TIMING UNCOMPRESSED MODE using the Thin Filter 1; the PN camera was not in operation. The source was outside the OM window, so these data were not used.

We analysed the data using the xmm-sas software v5.4.1. In TIMING MODE the central CCD data is compressed onto a single axis, thus selection is based on columns rather than pixels. Only single or double pixel events with a zero quality flag were selected from a 44-column region centred on the source. We also removed column 315 from the MOS-2 data, which showed a spurious signal at low energies. Owing to the limited coverage of the TIMING MODE window we used an adjacent chip (CCD3) to estimate the background.

The power spectrum of the 0.2–12 keV data from the MOS cameras is given in Fig. 1. This shows prominent peaks at the spin frequency and its first harmonic (periods 545.5 s and 272.7 s respectively). We find that the first harmonic is the stronger at energies below 0.7 keV (hereafter the ‘soft’ band), while the fundamental is the stronger at energies above 0.7 keV (hereafter the ‘hard’ band), as previously reported by Allan et al. (1996).

The folded lightcurves from the two bands (Fig. 2) confirm these results, showing that the soft emission has a double-peaked profile whereas the hard emission has a single-peaked, sawtooth modulation.

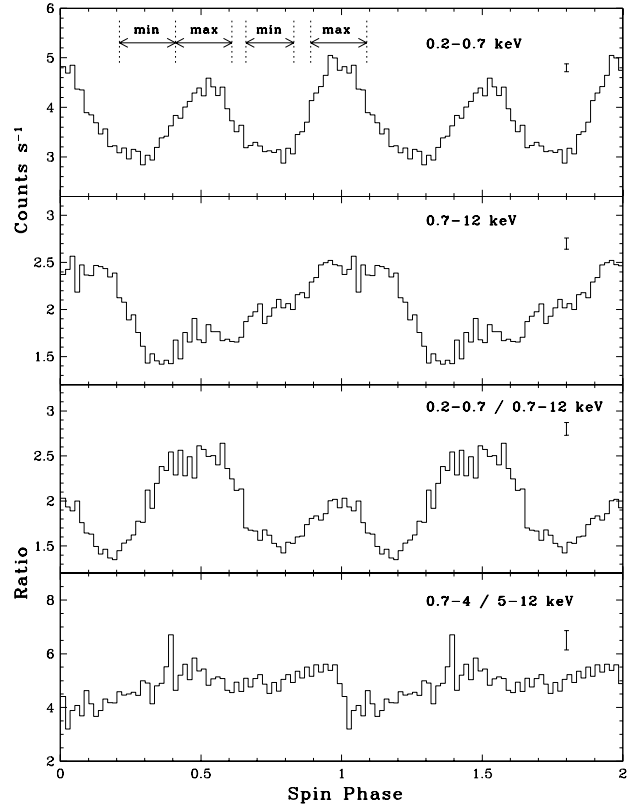


Figure 2. The X-ray data (MOS-1 + MOS-2) from the soft and hard bands (top panels), folded on the 545-s spin cycle. The lower panels contain the 0.2–0.7 / 0.7–12 keV and 0.7–4 / 5–12 keV softness ratios. Typical error bars are shown. Phase zero is taken as the peak of the larger of the soft maxima, and corresponds to HJD 2452187.55904.

3 SPECTROSCOPY

Little TIMING MODE data has yet been published, and we used pre-release versions of new quantum efficiency calibration files and canned response matrices (Sembay, private communication). However, there were clear calibration discrepancies between the two EPIC-MOS instruments below 0.4 keV (Fig. 3). We thus added systematic errors of 8% to the data in this energy range. Other than this, we do not make allowance for calibration uncertainties in calculating χ^2 values. The data from the two cameras were fitted simultaneously in the fits reported below.

The X-ray emission in an IP arises from plasma heated to X-ray temperatures at a stand-off accretion shock, which then cools as it approaches the white dwarf surface (e.g. Aizu 1973; Cropper et al. 1999). The CEMEKAL model reproduces a multi-temperature spectrum, with a power-law distribution of temperatures, based on the MEKAL plasma model.

Fitting our phase-averaged spectrum with a CEMEKAL model plus simple and partial-covering absorption (as commonly found in IPs) gave a poor fit ($\chi^2_\nu=20$) owing to a large soft excess. Adding a blackbody emitter to model the soft emission improved the fit hugely to $\chi^2_\nu=1.38$.

We then tried replacing the CEMEKAL with two MEKAL components and found a significant improvement in fit quality ($\chi^2=1276$, $\chi^2_\nu=1.28$) implying that a power-law is a poor

Component	Parameter (Units)	Value	Error
Absn.	n_{H} (cm $^{-2}$)	1.06×10^{21}	(+0.09, -0.12)
Blackbody	kT (keV)	3.97×10^{-2}	(+0.38, -0.42)
	Normalisation	1.34×10^{-2}	(+1.64, -0.79)
Absn	n_{H} (cm $^{-2}$)	2.06×10^{21}	(+0.29, -0.29)
Part. Absn.	n_{H} (cm $^{-2}$)	6.08×10^{22}	(+0.58, -0.52)
	CvrFract	0.52	(+0.03, -0.03)
Gaussian	Energy (keV)	6.42	(+0.02, -0.02)
	Normalisation	1.96×10^{-5}	(+0.44, -0.45)
	Eq. Width (eV)	121	(+27, -28)
Mekal	kT (keV)	0.168	(+0.008, -0.003)
	Abundance	3.39×10^{-2}	(+1.14, -0.62)
	Normalisation	0.32	(+0.16, -0.12)
Mekal	kT (keV)	9.00	(+0.92, -0.73)
	Abundance	0.12	(+0.35, -0.36)
	Normalisation	1.31×10^{-2}	(+0.08, -0.08)

Table 1. Model components and parameters fitted to the phase-averaged spectrum (see Section 3). The errors are the 90% confidence errors according to formal statistics (to the same power of ten as the values); note however that these are likely underestimates, since they do not account for the calibration systematics.

description of the temperature distribution in the plasma column. The best-fitting temperatures were 0.2 and 9 keV. The blackbody component was still necessary ($\chi^2_{\nu}=1.60$ without it), as were both simple and partial-covering absorption ($\chi^2_{\nu}=1.71$ without these). There were significant residuals at the 6.4-keV iron fluorescence line, so we added a narrow Gaussian component, reducing χ^2 to 1203 ($\chi^2_{\nu}=1.21$).

In the above models the simple and partial-covering absorbers acted on all of the emission components. However, the partial-covering absorber is sufficiently dense as to completely block any blackbody emission that it covers, thus its effect is redundant with a change in blackbody normalisation. So as a final tweak we altered the model so that the blackbody was only absorbed by a simple absorber, which, for generality, was allowed to have a different column than the absorber acting on the MEKALS. This yielded a slight χ^2 improvement ($\chi^2=1187$, $\chi^2_{\nu}=1.19$).

The resultant model is given in Table 1 and illustrated in Fig. 4. Note that the spectral parameters vary over spin phase, so those listed in Table 1 will be weighted averages.

4 PHASE-RESOLVED SPECTROSCOPY

We have found that below 0.7 keV the spectrum is dominated by a blackbody component, whereas above 0.7 keV the spectrum is dominated by optically thin plasma (Section 3). Further, the soft blackbody component is double-peaked over the spin cycle, whereas the higher-temperature plasma has a single-peaked, sawtooth pulse profile (Fig. 2). Thus, for phase-resolved spectroscopy, it makes sense to deal with the soft pulse and the hard pulse separately.

4.1 The soft pulse

To analyse the soft pulse we defined phase regions encompassing the maxima (phases 0.41–0.61 and 0.89–1.09) and

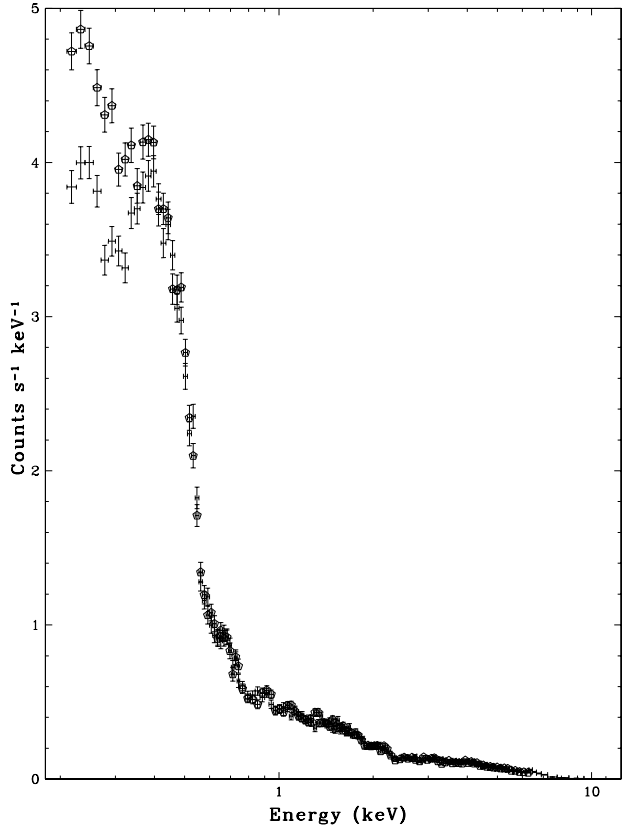


Figure 3. The phase-averaged spectra from the MOS-1 and MOS-2 (circles) cameras. The systematic discrepancy below 0.4 keV is clear.

minima (phases 0.21–0.41 and 0.66–0.83), as illustrated in Fig. 2.

We fitted all four phase regions simultaneously with the model developed above (Section 3), which comprised a soft blackbody and two MEKAL emitters, with a simple absorber acting on the blackbody, and both simple and partial-covering absorbers acting on the MEKAL emitters. For analysing the soft pulse the fits were allowed to optimise for the entire spectrum, but the quoted χ^2 values were calculated only from 0.2–0.7 keV (the changes in χ^2 between models were similar if χ^2 was calculated over the entire energy range).

Allowing the model to optimise for each phase region separately yielded a best-fitting χ^2 of 263 ($\chi^2_{\nu}=1.27$). Constraining the simple absorber to be the same at all phases caused minimal change in fit quality but reduces the number of free parameters ($\chi^2=264$, $\chi^2_{\nu}=1.25$).

Alternatively, allowing the absorption to vary freely, but forcing the blackbody emitter to remain constant between phase regions, yielded a χ^2 of 308.51 ($\chi^2_{\nu}=1.44$). This increase suggests that the soft modulation is a change in blackbody normalisation rather than a change in absorption.

Note that the 0.2–0.7 keV region is the worst affected by calibration uncertainties, so the quoted χ^2 values are unreliable. However, if we fit the data from each camera separately, without adding systematic uncertainties, we reach the same conclusion: that the soft pulse is mainly a change in visible emitting area, and not a change in absorption.

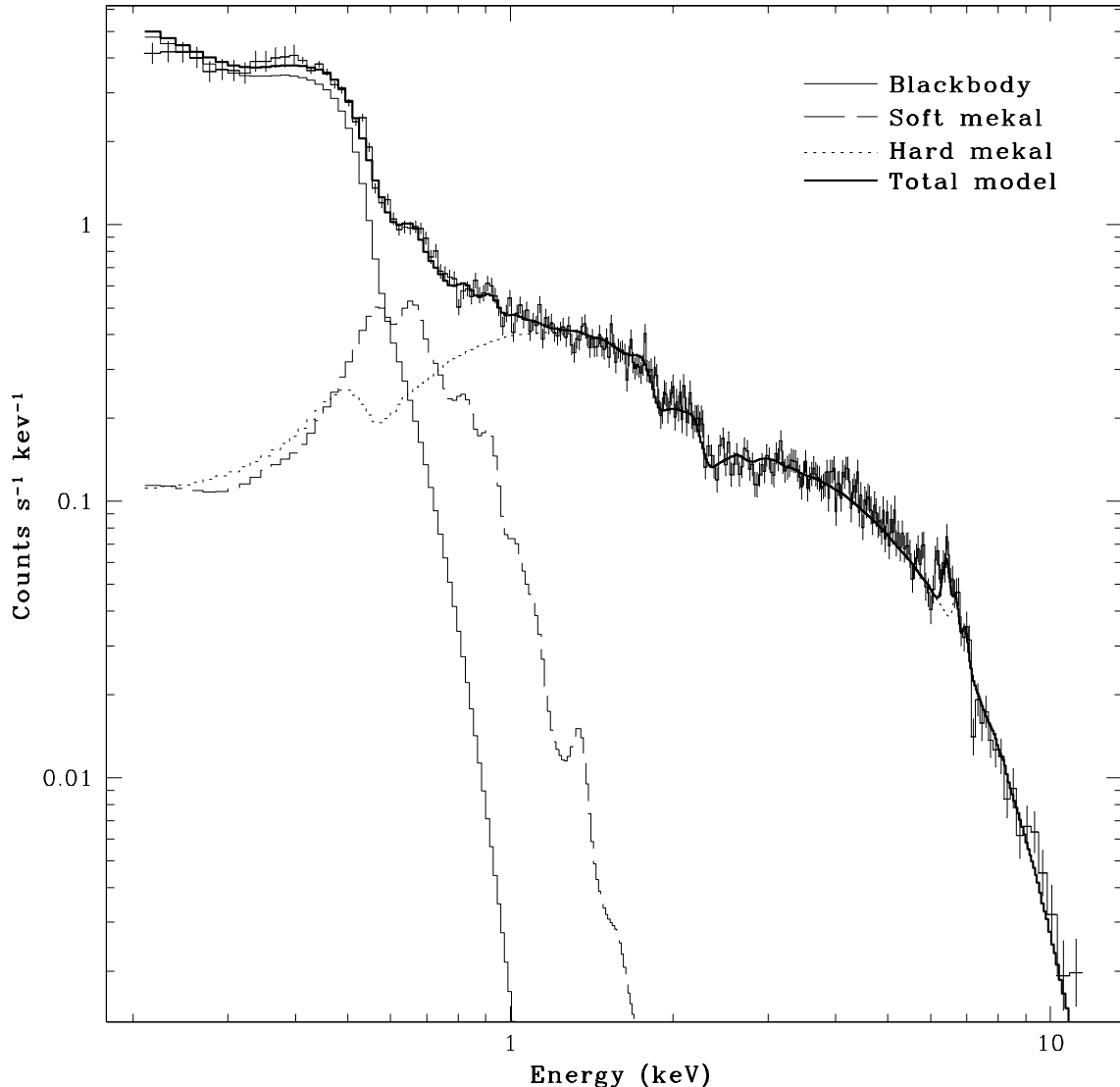


Figure 4. The phase-averaged spectrum with the fitted model, and the contributions from each component.

4.2 The Hard Pulse

Since the 0.2–0.7 / 0.7–12 keV softness ratio is effectively a ratio of the blackbody emission to the plasma emission, we have also computed the 0.7–4 / 5–12 keV softness ratio, which is sensitive to spectral changes in the harder plasma emission.

This ratio (Fig. 2) shows little variation other than a hardening at phases ~ 0.0 –0.2, near the maximum of the hard pulse. We thus extracted and compared spectra for the phase regions 0.0–0.2 and 0.4–0.9.

Fitting the model to the two phase regions independently gave a total χ^2 of 1253 ($\chi^2_\nu=1.10$; in this section χ^2 values are for energies above 0.7 keV only; again, this does not affect the $\Delta\chi^2$ values). Constraining the absorption (simple and partial covering) to have the same value in each phase region gave an identical χ^2 of 1253, implying no absorption change. Alternatively, requiring the normalisations of the MEKALs to be the same in each region worsened χ^2 to 1530 ($\chi^2_\nu=1.34$).

Thus we conclude that the hardening near flux maximum is caused by a change in the ratio of the soft and hard MEKAL components. At all other phase regions there appears to be little or no change in the ratios of the two MEKAL components, nor in the absorption. This is despite the fact that the overall flux level changes considerably over these phase regions. Similar results, that the hard pulse does not show much energy dependence, were reported using *BeppoSAX* data by de Martino et al. (2004).

5 DISCUSSION

V405 Aurigae has two main spectral components in the X-ray band. Below 0.7 keV the spectrum is dominated by a blackbody component which shows a double-peaked modulation over the spin cycle. Above 0.7 keV it is dominated by thermal plasma emission which has a single-peaked, saw-tooth modulation over the spin cycle.

IP X-ray modulations are often the result of absorp-

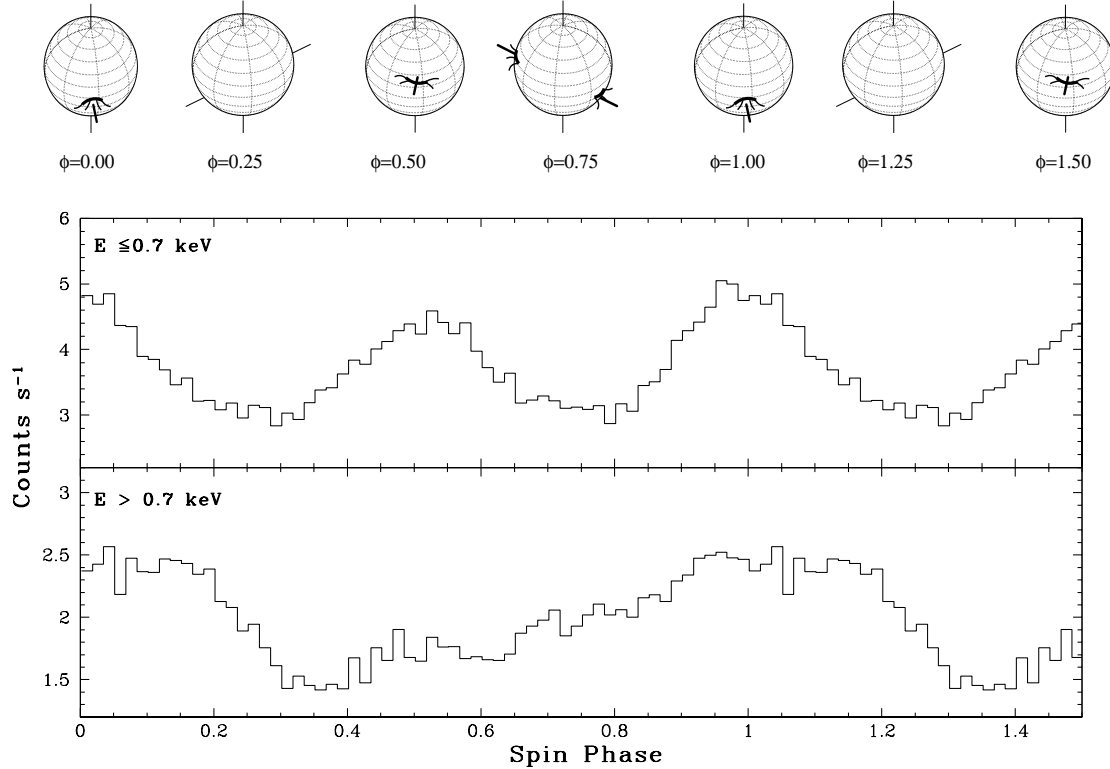


Figure 5. Schematic diagram showing the location of the emitting regions and magnetic poles at various phases. The dipole offset has been exaggerated. The arc-shaped regions are the blackbody emitting areas and the short lines depict the accreting field lines.

tion as ‘accretion curtains’ of material sweep across the line of sight with the spin cycle (e.g. Hellier, Cropper & Mason 1991; Kim & Beuermann 1995). Further, it has been proposed that whether the pulsation is single-peaked or double-peaked depends on whether the accretion column is short and fat, with greater horizontal opacity, or tall and thin, with greater vertical opacity (Hellier 1996; Allan et al. 1996; Norton et al. 1999).

V405 Aur, however, does not fit the above model since, firstly, it shows both single-peaked and double-peaked behavior in the same star. Secondly, our spectral modelling shows that the absorption varies little over spin phase (Section 3), which is the essence of the above model.

5.1 Explaining the spin pulse

We suggest that the modulation of the blackbody emission is simply the foreshortening of the accreting polecaps, which are viewed face on when a pole points towards us (maximum) and foreshortened when the pole is near the white dwarf limb (minimum). Thus one of the poles is in the middle of the visible face at each maximum (see Fig. 5). The difference between the two maxima is slight, so we require that both accretion polecaps be near the equator of the white dwarf, so that there is little difference in their visibility. This implies that the angle between the magnetic and spin axes

is large, as is also suggested by the polarimetry reported by Shakhovskoj, Andronov & Kolesnikov (2001).

Turning now to the hard X-ray pulse, the accretion geometry for a highly inclined dipole is illustrated in Fig. 6. This shows that the difference in view between the accretion footprints at the upper and lower poles is relatively small. Nevertheless, we can adopt the standard accretion-curtain model (see, e.g., Hellier et al. 1991) and suppose that the lower pole viewed at phase 0 is brighter than the upper pole viewed at phase 0.5 (Fig. 6). This is because the opacity in the column causes X-rays to emerge preferentially perpendicular to the curtain, which means that the lower pole is somewhat better presented.

Note that with such a high dipole inclination, the cooler, outer regions of the accretion curtains never cross the line of sight. This explains why we don’t see a prominent absorption dip dominating the spin pulse, in contrast to many other IPs (e.g. AO Psc, Hellier et al. 1991). However, the X-rays will be emerging from a highly ionized post-shock region in which absorption and electron scattering will cause opacity, thus explaining the change in brightness with aspect of the accretion curtain, and the need for a partial-covering absorber in the spectral fit.

Note that at phase 0 the blackbody emission seen at the lower pole would be from heated surface on the side of the curtain further from the magnetic pole (that nearer the

pole being obscured by the curtain) whereas at phase 0.5 the blackbody emission at the upper pole is from the side nearer to the magnetic pole (see Fig. 6). Thus an asymmetry between these regions can explain the fact that one maximum is higher than the other.

5.2 The sawtooth profile

We further need to explain the fact that the hard-X-ray pulse shows a sawtooth profile, declining more rapidly than it rises. We suggest that this can be explained if the magnetic dipole is offset by $\sim 0.1\text{--}0.2$ white-dwarf radii. Such offsets are commonly found in magnetic white dwarfs (Wickramasinghe & Ferrario 2000).

From the deductions above, the lower pole is on the meridian facing us at phase 1 (thus presenting maximum blackbody area and producing a soft maximum). However, suppose that the dipole is offset to the left (Fig. 5), so that the magnetic pole only points towards us shortly afterwards. This will slightly delay the hard X-ray peak.

The lower pole then disappears over the limb at phase 0.25. Because of the offset, the upper pole does not yet appear, and this asymmetry explains the relatively rapid fall in flux at this phase.

With the asymmetry pushing both poles to the far side of the white dwarf, we have lowest flux occurring before 0.5. Then the upper pole appears and is in the middle of the face near phase 0.5. Its less favorable aspect makes the system fainter than when we see the lower pole at phase 1.0.

As we continue through the cycle towards phase 0.75, the offset of the dipole biases both poles towards the visible face of the white dwarf, which is why we see more flux approaching phase 0.75 than we do following phase 0.25, thus explaining the sawtooth. However, since both accretion curtains are then presented with their azimuthal sweep being edge on to us, the flux level is lower than at phase 1.0.

5.3 The optical spin pulse

Although we do not present optical data in this paper, we can consider whether the model can explain the double-peaked nature of the optical spin pulse (e.g. Allan et al. 1996; Skillman 1996; Still, Duck & Marsh 1998).

In the standard accretion-curtain model, with a relatively low dipole inclination, the changing visibility of the curtains results in a single-peaked pulse with a maximum when the upper pole points away from us (Hellier et al. 1991; Kim & Beuerman 1996).

However, in V405 Aur we are postulating a large dipole inclination, such that the accretion curtains are nearly flat in the orbital plane (Fig. 6). Note that this is also supported by the optical polarimetry of Shakhovskoj et al. (2001) which implies equal visibility of two poles near the equator.

With accretion curtains nearly in the plane, the view when the upper pole points towards us is similar to that when the lower pole points towards us (Fig. 6). Thus we can explain a double-peaked optical pulse if the curtains are brighter when one of the poles points towards us and fainter when both are at quadrature (or vice versa).

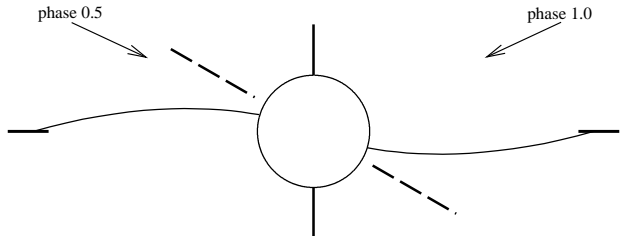


Figure 6. Side-on schematic view of the model proposed in the text, shown here for a system inclination of 65° and a dipole inclination of 60° .

5.4 The blackbody emitting area

From our spectral fits we can estimate the blackbody emitting area. Note, however, that the calculated blackbody flux is strongly dependent upon the degree of absorption acting on it. In our best fitting model (Table 1) this is surprisingly large ($\sim 10^{21} \text{ cm}^{-2}$), particularly if we associate the simple absorber with interstellar absorption. This in turn causes the flux measured to be high. However, forcing the column density to take on a lower value (e.g. $3 \times 10^{20} \text{ cm}^{-2}$) causes a worsening in χ^2 of $\gtrsim 100$. Note, though, that the energy range over which the absorbed blackbody acts is that for which the calibration uncertainties are at their worst, making the values unreliable. In what follows we use the flux calculated from the best fit ($n_H = 10^{21} \text{ cm}^{-2}$).

The blackbody emission component (Section 3) has an unabsorbed bolometric flux of $1.12 \times 10^{-12} \text{ J m}^{-2} \text{ s}^{-1}$ with a temperature of 40 eV. This implies an emitting area of $4.76 \times 10^5 (d/300 \text{ pc})^2 \text{ km}^2$, which corresponds to $\sim 8 \times 10^{-4}$ of a white-dwarf surface [Haberl & Motch (1995) reported a corresponding value of 2×10^{-5} , based on a temperature of 57 eV and a column of $5.7 \times 10^{20} \text{ cm}^{-2}$.] This area is consistent with other estimates for the accretion area in IPs, for example the upper limit of 0.002 deduced by Hellier (1997) from eclipse timings of XY Ari.

6 CONCLUSIONS

XMM-Newton observations of V405 Aur confirms that the soft X-rays are dominated by a blackbody component, presumably from heated white-dwarf surface surrounding the accretion regions. The heated region covers $\sim 8 \times 10^{-4}$ of the white dwarf, comparable to the upper limit found from eclipse timings of XY Ari.

We propose that the modulation of this component results from foreshortening of the blackbody emitting regions. We view the heated surface most favourably when either pole points towards us, so we see a double-peaked modulation in soft X-rays. The equality of the two maxima requires that the magnetic axis be highly inclined from the spin axis.

The hard X-ray emission shows a single-peaked, sawtooth modulation. This does not show the strong energy dependence of absorption, as usual in IPs. We suggest that this is because, with the high dipole inclination, the outer parts of the accretion curtains never cross the line of sight. However, electron scattering and opacity in the highly ionized post-shock column causes the intensity variation with spin phase. The sawtooth shape of the pulsation requires

that the magnetic axis be offset from the white-dwarf centre.

We also suggest that the high dipole inclination is responsible for the double-peaked optical pulse. The high dipole inclination appears to be the main reason for the differences between V405 Aur's pulsation and typical IP behaviour.

ACKNOWLEDGEMENTS

The observation reported here was performed by Leicester University, who also constructed the MOS cameras and developed the analysis software. In particular we thank Steve Sembay and Richard Saxton for their help in overcoming calibration difficulties, and for providing us with the latest pre-release CCF and RMF files for use in this analysis. We also thank Liza van Zyl and Gavin Ramsay for some illuminating discussions.

REFERENCES

Allan A., Horne K., Hellier C., Mukai K., Barwig H., Bennie P.J., Hilditch R.W., 1996, MNRAS, 279, 1345
 Aizu K., 1973, Prog. Theor. Phys., 49, 1184
 Cropper M., Wu K., Ramsay G., Kocabiyik A., 1999, MNRAS, 308, 807
 de Martino D., Matt G., Belloni T., Haberl F., Mukai K., 2004, A&A, 415, 1009
 Haberl F., Thorstensen J.R., Motch C., Schwarzenberg-Czerny A., Pakull M., Shambrook A., Pietsch W., 1994, A&A, 291, 171
 Haberl F., Motch C., 1995, A&A, 297, L37
 Hellier C., 1996, in Evans A., Wood J.H., eds, Cataclysmic Variables and Related Objects, Kluwer Academic Publishers, Dordrecht, p. 143
 Hellier C., 1997, MNRAS, 2291, 71
 Hellier C., 2001, Cataclysmic Variable Stars, Springer-Praxis, Chichester, UK
 Hellier C., Cropper M., Mason K., 1991, MNRAS, 248, 233
 Jansen F. et al., 2001, A&A, L1
 Kim Y., Beuermann K., 1995, A&A, 298, 165
 Kim Y., Beuermann K., 1996, A&A, 307, 824
 Kuijpers J., Pringle J.P., 1982, A&A, 114, L4
 Norton A.J., Beardmore A.P., Allan C., Hellier C., 1999, A&A, 347, 203
 Patterson J., 1994, PASP, 106, 209
 Shakhovskoj N.M., Andronov I.L., Kolesnikov S.V., 2001, AGM, 18, 16
 Skillman D.R., 1996, PASP, 108, 130
 Still M.D., Duck S.R., Marsh T.R., 1998 MNRAS, 299, 759
 Turner M.J.L. et al., 2001, A&A, 365, L27
 Wickramasinghe D.T., Ferrario L., 2000, PASP, 112, 873